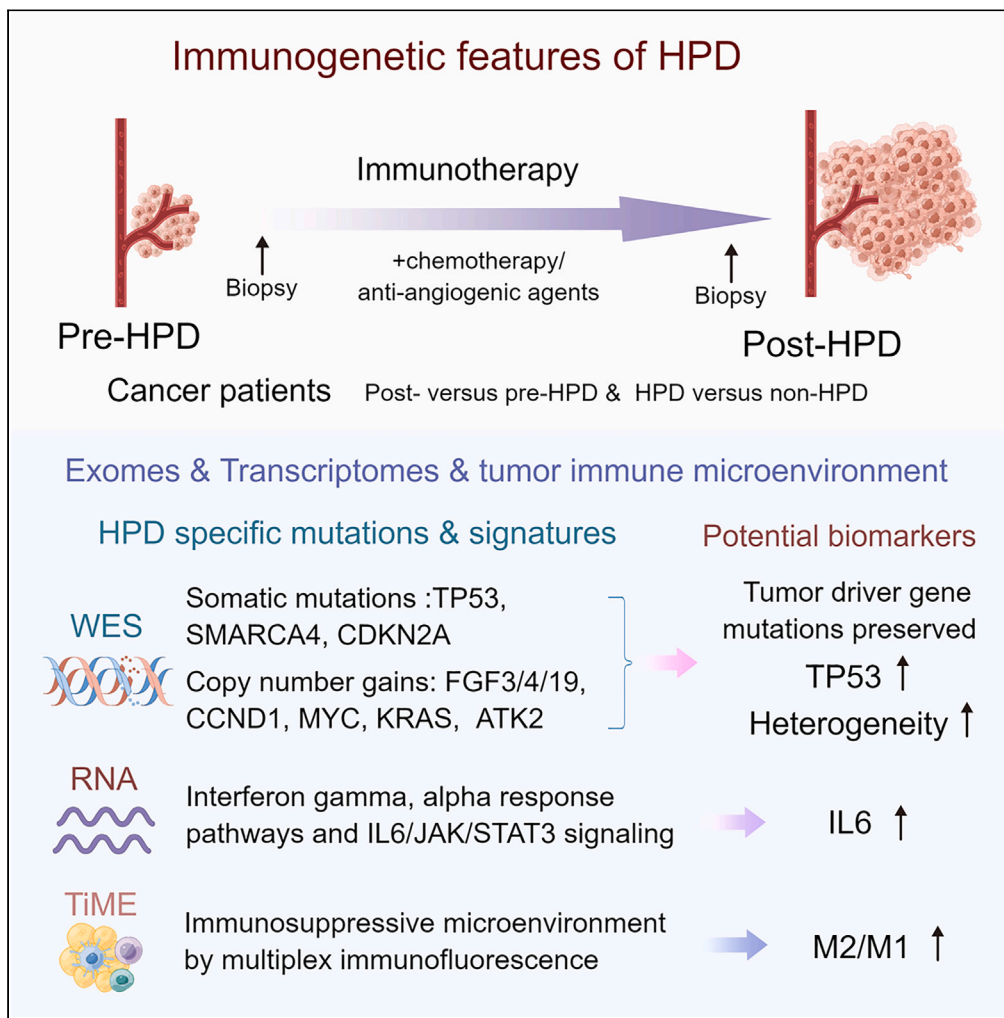


Article

Exploration of the immunogenetic landscape of hyperprogressive disease after combined immunotherapy in cancer patients



Caifeng Gong,
Wen Zhang,
Yongkun Sun, ...,
Jun Liu, Ying Sun,
Aiping Zhou

aiping_zhou@yeah.net

Highlights
Immunogenetic changes in hyperprogressive disease after combined immunotherapy

The driver genetic variations of patients after hyperprogressive disease kept stable

Increased IL-6 expression and higher tumor heterogeneity might be crucial

Repressed tumor immune microenvironment with increased M2/M1 macrophage ratio

Gong et al., iScience 26, 106720
June 16, 2023 © 2023 The Authors.
<https://doi.org/10.1016/j.isci.2023.106720>



Article

Exploration of the immunogenetic landscape of hyperprogressive disease after combined immunotherapy in cancer patients

Caifeng Gong,¹ Wen Zhang,¹ Yongkun Sun,¹ Jianzhong Shou,² Zhichao Jiang,¹ Tianyi Liu,¹ Shengzhou Wang,³ Jun Liu,³ Ying Sun,³ and Aiping Zhou^{1,4,*}

SUMMARY

The immune-genetic changes that occur in cancer patients experiencing hyperprogressive disease (HPD) during combined immunotherapy are unclear. In this study, HPD patients with pre- and post-HPD samples and non-HPD patients with solid tumors were molecularly characterized by genetic and tumor immune microenvironment (TiME) analyses of paired samples by whole-exome sequencing, RNA sequencing, and multiplex immunofluorescence. The genetic analysis of paired samples showed that almost all the tumor driver gene mutations were preserved between pre- and post-HPD tumors. HPD patients had higher frequencies of mutations in *TP53* and *CNN2*, and a significantly higher mutant-allele tumor heterogeneity than non-HPD patients. Tumor IL-6 mRNA was upregulated in post-HPD samples vs. pre-HPD, accompanied by a potential immune suppressive TiME with an elevated M2/M1 ratio. Salvage treatment with irinotecan plus bevacizumab was effective in one HPD patient, who experienced prolonged survival. These genetic features and TiME characteristics might help identify the features of HPD after immunotherapy.

INTRODUCTION

Immune checkpoint blockade (ICB) has been one of the most important breakthroughs in oncology in the last decade. Since the approval of ipilimumab for advanced melanoma in 2010, the Food and Drug Administration (FDA) has approved the treatment of immune checkpoint inhibitors (ICIs) for over 20 malignant tumor types or disease indications. However, an unexpected rapid acceleration of cancer progression shortly after the initiation of ICB, referred to as hyperprogressive disease (HPD), occurs in some patients; HPD can be devastating and has attracted substantial attention from physicians and researchers.¹ There is still no unified definition for HPD. Nevertheless, it is generally accepted that HPD meets the following criteria: tumor burden increase >50%, tumor growth rate (TGR) > 2-fold, and time to treatment failure (TTF) < 2 months.² The reported HPD incidence during ICB monotherapy varies from 4% to 29%, depending on tumor types and definitions of HPD.^{3,4} When an ICI is combined with chemotherapy or a target agent, the incidence rate of HPD is somewhat lowered but remains significant.^{5,6}

Several clinical and genetic features are associated with HPD, such as older age, poor performance status, higher tumor burden, MDM2/MDM4 amplification, and epidermal growth factor receptor (EGFR) alterations.^{1,3,7–10} Additionally, the tumor immune microenvironment (TiME), with enhanced infiltration of programmed cell death protein 1 (PD-1)-positive regulatory T cells and M2-like macrophages, was recently recognized as a promoter of HPD in patients receiving immunotherapy based on tumor cell-intrinsic PD-1 expression.^{11–15} However, most studies on HPD have explored baseline samples in monotherapy. What happens to the immunogenetic changes after HPD associated with combined immunotherapy, one of the most popular treatment strategies, is rarely reported; therefore, we conducted this comparison analysis study to better understand the biological process of HPD.

In this study, we performed whole-exome sequencing (WES), RNA sequencing (RNA-seq), and multiplex immunofluorescence (mIF) to identify the immunogenomic features associated with HPD tumors after combined immunotherapy by comparing the genetic profiles and the potential TiME landscapes with pre- and

¹Department of Medical Oncology, National Cancer Center/National Clinical Research Center for Cancer/Cancer Hospital, Chinese Academy of Medical Sciences and Peking Union Medical College, Beijing 100021, China

²Department of Urology, National Cancer Center/National Clinical Research Center for Cancer/Cancer Hospital, Chinese Academy of Medical Sciences and Peking Union Medical College, Beijing 100021, China

³GenomiCare Biotechnology Co. Ltd, Shanghai 201203, China

⁴Lead contact

*Correspondence:

aiping_zhou@yeah.net

<https://doi.org/10.1016/j.isci.2023.106720>



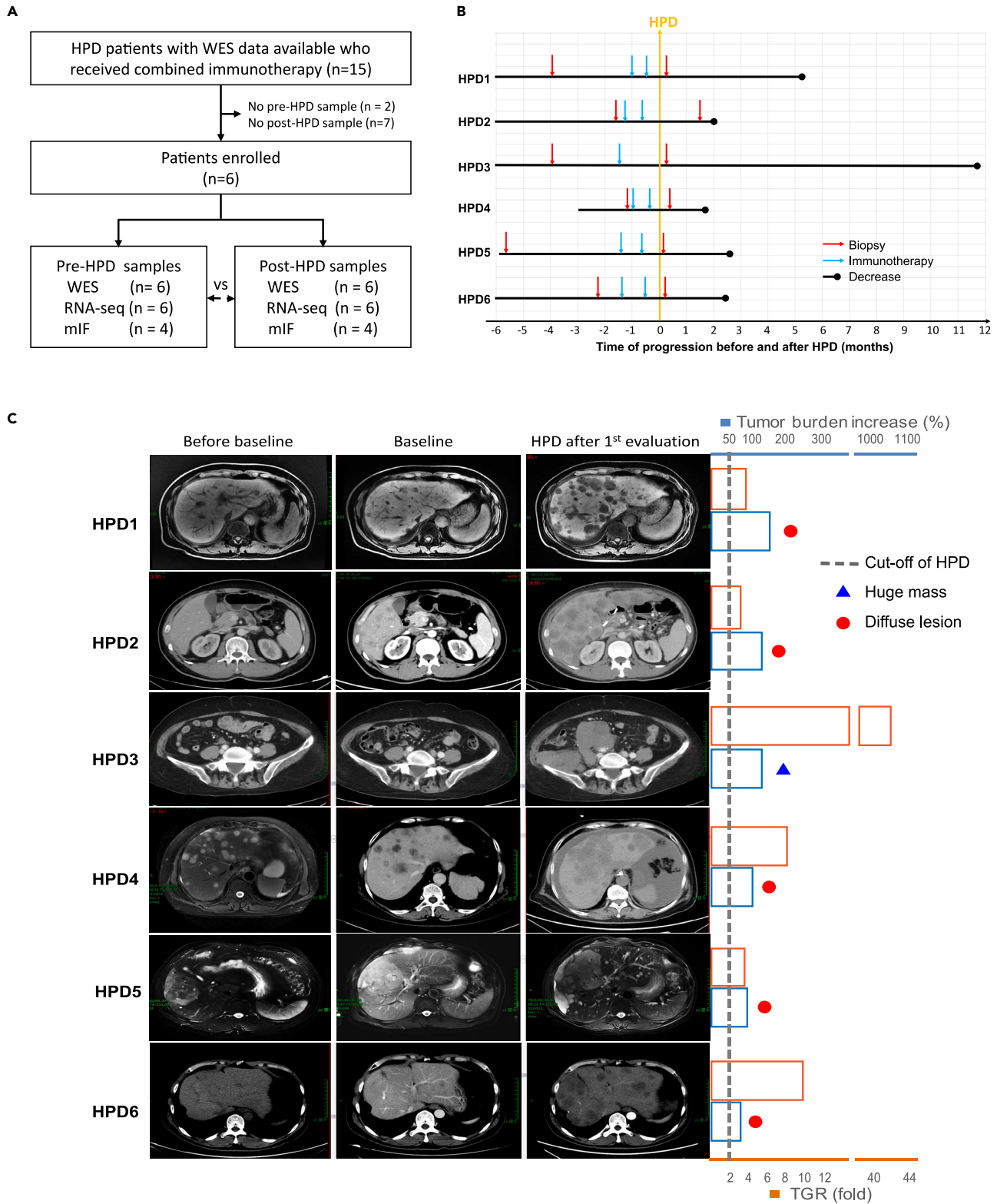


Figure 1. Clinical characteristics of the HPD patients and study design

(A) Patient inclusion criteria and study design.

(B) Schematic timeline of relevant clinical events in 6 HPD patients.

Figure 1. Continued

(C) Representative images from 6 HPD patients before treatment, at baseline, and at the first evaluation post-treatment. Tumor burden increase (blue bars), tumor growth rate (TGR: orange bars), and occurrence of new lesions (red dot or blue triangle) are labeled on the right graph. The gray dashed line represents the cutoff value of the definition for HPD. PD-1, programmed cell death protein 1; PD-L1, programmed cell death-ligand 1; HPD, hyperprogressive disease; WES, whole-exome sequencing; RNA-seq, RNA sequencing; mIF, multiplex immunofluorescence; TGR: tumor growth rate.

post-HPD paired samples. Our findings are potentially useful for elucidating the probable biological process of HPD.

RESULTS**Patient characteristics**

Candidate patients received anti-PD-1/PD-L1 combination treatment and HPD was defined as previously reported.² A total of 15 HPD patients with WES data available who received combined immunotherapy were screened, and 6 patients with paired pre- and post-HPD samples were included in the final analysis (Figures 1A and 1B). The patient characteristics are described in Table 1. The median age of HPD patients was 56.0 (range: 49.0–67.0) years. The patient samples were mainly from the digestive system, including 2 hepatobiliary tumors, 2 gastroesophageal cancers, 1 uroepithelial carcinoma, and 1 thymic carcinoma. Three of the patients received immunotherapy (anti-PD-1) combined with chemotherapy (1 carboplatin, 1 albumin paclitaxel, and 1 irinotecan) and 3 received immunotherapy combined with anti-angiogenic agents (2 anlotinib plus anti-PD-L1 and 1 bevacizumab plus anti-PD-1). At the first post-treatment evaluation, the HPD patients' tumor burden increased by 78.7%–157.8%, and the TGR increased by 3.2- to 41.7-fold compared to the corresponding indices at the reference period before starting immunotherapy with an explosive pattern (Figure 1C). After immunotherapy, massive new lesions developed in one patient (HPD3), and diffuse new lesions developed in the other 5 patients. Besides, 83.3% (5/6) of post-HPD samples were taken from the same site to pre-HPD, including 2 primary lesions (liver) and 3 metastatic lesions (metastatic lymph nodes).

Genetic analysis of paired HPD patient samples

We conducted somatic mutation profiling to explore the genetic features associated with HPD using WES data of paired pre-versus post-HPD samples. A total of 5,671 somatic mutations including 1,481 nonsilent mutations (1,340 point mutations and 141 indels) and 4,190 silent mutations were identified across the 12 tumor samples. The number of mutations was comparable across patients, and the median numbers of somatic mutations in post-HPD samples (range: 85–153, median: 121.5) were similar to those in pre-HPD samples (range: 100–166, median: 117.5), with no obvious differences ($p = 0.753$, Figure 2A). However, tumor samples from the same patient shared variable percentages of total somatic mutations (range: 27.5–50.4%, median: 39.1%, Figure S1A). Tumor driver gene mutations were more likely to affect tumor progression and there were few changes after HPD (Figure 2B and Table 2). Nearly all the tumor driver single nucleotide variation (SNV) in pre-HPD samples were preserved in the post-HPD samples, including *TP53*, *SMARCA4*, and *CDKN2A*. Genes with potential driver copy number (CN) gains shared in paired pre- and post-HPD samples, included *FGF3/4/19*, *CCND1*, *MYC*, *KRAS*, and *ATK2*. These genes are widely known to participate in cell proliferation, the cell cycle, and interference with tumor suppressors. Several genes were commonly altered in different patients, and somatically altered genes shared among at least 3 patients in both pre- and post-HPD samples were *TP53* (mutations in 6 pre-HPD samples and 6 post-HPD samples, presented as 6/6), *TTN* (4/4), and *CNN2* (4/3) (Figure 2C). Mutations in *TTN* were likely passenger events as it is one of the longest human genes. Mutations in *TP53* were shared among all paired samples from 6 patients, and all mutation sites were inside the DNA-binding domain (DBD) of the p53 protein (Figure S1B). The mutations in *TP53* were predicted to be likely deleterious based on the combined annotation-dependent depletion (CADD) scores¹⁶ (Table S1). The shared mutations appeared to form the trunk based on the clonal evolution of tumors (Figure S1C).

Tumor mutation burden (TMB) is associated with clinical response to ICI therapy in several other cancer types. However, the impact of the TMB on HPD occurrence with immunotherapy remains less characterized. We did not find a significant change between pre- and post-HPD samples ($p = 0.844$, Figure 2D), and the median TMB of pre-HPD samples assessed by WES was 3.47 mut/Mb (range: 2.43–4.37), while the TMB of post-HPD was 3.36 mut/Mb (range: 2.86–4.74). Tumor heterogeneity potentially influences treatment efficacy and prognosis. Mutant-allele tumor heterogeneity (MATH) scores were calculated using WES data to evaluate tumor heterogeneity. MATH scores were numerically decreased in post-HPD

Table 1. Characteristics of HPD patients

Characteristics	HPD1	HPD2	HPD3	HPD4	HPD5	HPD6
Age (years)	59	49	67	59	53	47
Sex	Female	Male	Female	Female	Male	Male
Cancer type	Thymic carcinoma	Esophageal cancer	Urothelial carcinoma	Stomach cancer	Hepatocellular carcinoma	Hepatocellular carcinoma
Type of ICI	PD-1	PD-1	PD-1	PD-1	PD-L1	PD-L1
ICI combined strategy	Anti-angiogenesis	Chemotherapy	Chemotherapy	Chemotherapy	Anti-angiogenesis	Anti-angiogenesis
ICI treatment lines	3	2	2	2	2	3
MSI status	MSS	MSS	MSS	MSS	MSS	MSS
PD-L1 mRNA expression (TPM)						
Pre-HPD	0.56	2.32	3.13	5.47	1.26	9.33
Post-HPD	0.47	0.86	5.36	4.92	3.95	13.91

HPD, hyperprogressive disease; ICI, immune checkpoint inhibitors; MSI, microsatellite instability; MSS, microsatellite stable; TPM: transcripts per million.

samples compared with pre-HPD samples, although the difference was not significant (median: 68.0 vs. 82.4, $p = 0.438$, [Figure 2E](#)).

We also investigated copy number alterations (CNAs) in paired pre- and post-HPD samples. A total of 10483 CNAs, including 7983 copy number gains ($CN \geq 3,4617$ in pre-HPD and 3,366 in post-HPD) and 2,500 deletions ($CN \leq 1.2$, 1210 in pre-HPD and 1290 in post-HPD), were identified in 6 paired samples. There was no significant change in total CNAs in post-HPD compared with pre-HPD samples after combined immunotherapy ($p = 0.753$, [Figure S2](#)). The median copy number gains in pre- and post-HPD samples were 809 (range: 303–1271) and 569.5 (range: 83–1049), respectively. The median copy number deletions were 202.5 (range: 59–345) and 106.5 (range: 26–733), respectively. A quarter of these CNAs (range: 5.5%–46.5%, median: 24.7%) were shared in the pre- and post-HPD samples in one patient, and the shared percentage of copy number gains (range: 5.9%–50.4%, median: 25.6%) was higher than that of deletions (range: 4.1%–31.5%, median: 18.2%). Genes with CN gains shared in at least 3 patients in pre- and post-HPD samples included *MROH6* (5/4), *LGALS7* (5/4), *SLC52A2* (4/4), *ZFP36* (4/4), *ACTN4* (4/3), *CAPN12* (4/3), and *RXFP4* (4/3) ([Figure 2C](#)).

Gene expression and serum inflammatory factors of HPD patients

To better understand the molecular mechanism underlying HPD, we performed RNA-seq on HPD patients. All 6 paired samples passed quality control for further analyses. First, RNA-seq data were used to identify DEGs associated with HPD with a paired analysis of each patient's pre- and post-HPD sample. The results showed that 3 genes were upregulated after HPD, and 22 genes were downregulated ([Figure 3A](#), [Table S2](#)). In particular, interleukin-6 (IL-6), an immune- and inflammatory-related cytokine, was significantly upregulated in all 6 patients after HPD ($p = 0.031$, [Figure 3B](#)), suggesting the potential participation of this cytokine in HPD. Further, single sample gene set enrichment analysis (ssGSEA) identified several functions and/or pathways key to body immunity or biological processes, including glycolysis, PI3K/AKT/mTOR signaling, interferon gamma response, interferon alpha response, hypoxia, complement, and IL6/JAK/STAT3 signaling ([Figure 3C](#)). The analysis of immune subset features showed elevated follicular helper T cell levels by CIBERSORT and a decrease in natural killer (NK) cells and B cells by MCPCONTER in the post-HPD samples compared to the matched pre-HPD samples ([Figure S3](#)). We also investigated whether HPD tumors demonstrated changes in their capacity to elicit productive immune reactions using an in silico immunophenogram approach¹⁷; however, the post-HPD tumors had no significant differences in immunophenoscores compared with the pre-HPD tumors ([Figure S4](#)).

We additionally analyzed the changes in blood inflammatory factors after HPD, and the results showed that C-reactive protein (CRP) was significantly increased in post-HPD samples versus pre-HPD samples (median, 3.49 vs. 1.11 mg/L, $p = 0.043$, [Figure 3D](#)), but there was no significant change in the neutrophil-lymphocyte ratio (NLR, median, 3.55 vs. 3.23, $p = 0.600$, [Figure 3E](#)).

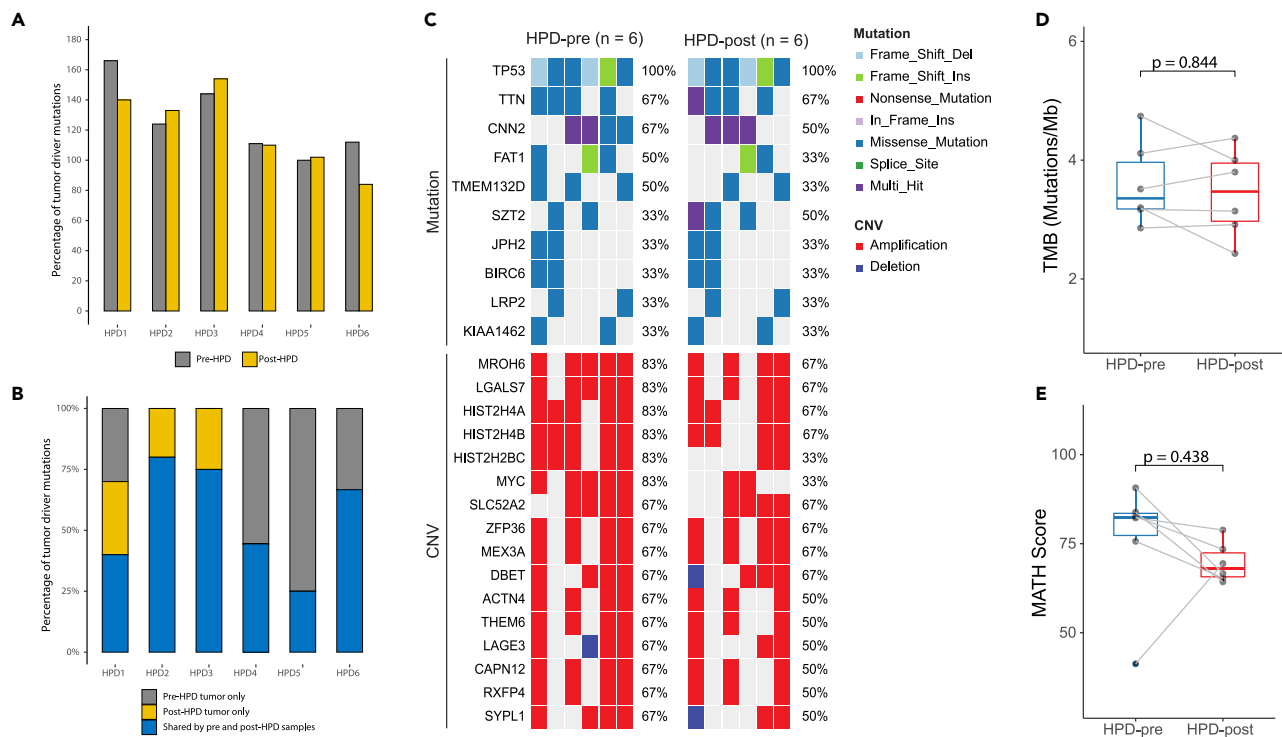


Figure 2. Genetic profiling of HPD patients by WES

(A) Somatic mutations in pre- and post-HPD samples in each patient.

(B) Percentage of tumor driver mutations shared by pre- and post-HPD samples and private to only pre- or only post-HPD samples in each patient.

(C) OncoPrint displaying the frequency of somatic mutated genes and copy number variations in HPD patients with pre-HPD and post-HPD samples.

(D) TMB of the paired pre- and post-HPD samples.

(E) MATH score of the paired pre- and post-HPD samples. HPD, hyperprogressive disease; WES, whole-exome sequencing; MATH, mutant allele tumor heterogeneity. The boxplot displays the standard five-number summary (Q1 – 1.5*IQR, Q1, Median, Q3 and Q3 + 1.5*IQR).

Tumor immune signatures *in situ* in HPD tumors

To investigate how body immunity against tumors was compromised when anti-PD-1/L1 agents were administered, we examined additional molecular features of TIME to gain further insight into cellular and spatial resolution by mIF. The panel of CK/CD8/CD68/CD163/PD-1/PD-L1 was designed to assess the tumor immune stroma contexture and the intrinsic PD-1/PD-L1 expression features on tumor cells in the TIME. Four paired samples were available and passed quality control for the final analysis. We found that the infiltration of M2 (CD68⁺CD163⁺) macrophages in the post-HPD samples was numerically greater than that in the pre-HPD samples in the tumor area (median density, 76.44 vs. 22.14 cells/mm² and median percentage, 1.54 vs. 0.30%) and in the stromal area (median density, 45.60 vs. 11.70 cells/mm² and median percentage, 1.19 vs. 0.30%, Figures 3F and 3G, Table S3). In contrast, the total number of CD8⁺ cells in the post-HPD samples was numerically lower than that in the pre-HPD samples. Interestingly, we compared the ratios between the median expression levels of immune-inhibiting M2 macrophages versus immune-promoting M1 macrophages (CD68⁺CD163⁻) and found that the M2/M1 ratio was higher in post-HPD samples (median 51.60) than in pre-HPD samples (median, 2.06) in the stromal area ($p = 0.068$, Figure 3H). No obvious change was observed in the expression of PD-L1 between pre- and post-HPD tumor cells (Table S3). Due to the limited sample size in these analyses, further validation is warranted.

Comparison of immunogenetic features between HPD and non-HPD patients

To better understand the genomic features and potential biomarkers associated with HPD, we next compared baseline somatic gene variations between HPD and non-HPD patients. A total of 51 patients with WES data who received immunotherapy were screened, and 24 non-HPD patients with baseline samples available were included in the final comparison analysis. Patient characteristics are described in Table S4. The HPD patients showed higher mutation frequencies of *TP53* (100% vs. 50%, $p = 0.057$) and *CNN2* (67% vs. 8%, $p = 0.007$), and a series of amplifications, as well as higher tumor heterogeneity scores (MATH score, 82.4 vs.

Table 2. Tumor driver gene alterations in paired samples of 6 HPD patients

Patient ID	Gene symbol	Gene variation	Mutation existence			Frequency/Copy number (VAF)		Variant Type	Signaling pathways/ Molecular mechanisms
			Pre-HPD	Post-HPD	Shared genes	Pre-HPD	Post-HPD		
HPD1	TP53	p.C242fs	Yes	Yes	Yes	77.51	61.94	SNV	TP53-inactivating
	AKT2	Gain	Yes	Yes	Yes	9.9	9.9	CNV	AKT2-activating
	CCNE1	Gain	Yes	Yes	Yes	5.56	5.53	CNV	CCNE1-amplification
	CDKN2A	Gain	Yes			3.35		CNV	CDKN2A-activating
	CDKN2B	Gain	Yes			3.72		CNV	CDKN2B-activating
	MCL1	Gain	Yes	Yes	Yes	3.96	3.28	CNV	MCL1-activating
	MYC	Gain	Yes			3.15		CNV	MYC-activating
	PALB2	p.K1048R		Yes			7.81	SNV	PALB2-unknown
	PIK3CD	Gain		Yes			3.64	CNV	PIK3CD-amplification
CCND2	Gain		Yes			3	CNV	CCND2-activating	
HPD2	TP53	p.I162F	Yes	Yes	Yes	84.47	85.55	SNV	TP53-inactivating
	CCND1	Gain	Yes	Yes	Yes	8.48	8.18	CNV	CCND1-activating
	CDKN2A	Loss	Yes	Yes	Yes	0.93	0.72	CNV	CDKN2A-loss
	CDKN2B	Loss	Yes	Yes	Yes	0.85	0.92	CNV	CDKN2B-loss
	FGF19	Gain	Yes	Yes	Yes	7.94	8.7	CNV	FGF19-activating
	FGF3	Gain	Yes	Yes	Yes	7.74	8.01	CNV	FGF3-activating
	FGF4	Gain	Yes	Yes	Yes	7.98	8.89	CNV	FGF4-activating
	SMARCA4	p.Q1480*	Yes	Yes	Yes	74.05	79.59	SNV	SMARCA4-inactivating
	EPHA3	Gain		Yes			3.53	CNV	EPHA3-amplification
RB1	Loss		Yes			1.16	CNV	RB1-inactivating	
HPD3	TP53	p.D259Y	Yes	Yes	Yes	91.39	92.09	SNV	TP53-inactivating
	CCNE1	Gain	Yes	Yes	Yes	3.11	3.9	CNV	CCNE1-amplification
	MYC	Gain	Yes	Yes	Yes	3.33	3.36	CNV	MYC-activating
	CDKN2A	Loss		Yes			1.2	CNV	CDKN2A-loss
HPD4	TP53	p.H214fs	Yes	Yes	Yes	30.06	52.25	SNV	TP53-inactivating
	CDKN2A	p.A76fs	Yes	Yes	Yes	29.24	63.01	SNV	CDKN2A-inactivating
	KRAS	Gain	Yes	Yes	Yes	9.9	4.25	CNV	KRAS-activating
	MYC	Gain	Yes	Yes	Yes	9.9	7.86	CNV	MYC-activating
	CCND1	Gain	Yes			3.65		CNV	CCND1-activating
	FGF19	Gain	Yes			3.29		CNV	FGF19-activating
	FGF4	Gain	Yes			3.42		CNV	FGF4-activating
	PALB2	p.S1084*	Yes			7.32		SNV	PALB2-unknown
RB1	Loss	Yes			1.2		CNV	RB1-inactivating	
HPD5	TP53	p.M237fs	Yes	Yes	Yes	63.44	31.38	SNV	TP53-inactivating
	MCL1	Gain	Yes			3.24		CNV	MCL1-activating
	MYC	Gain	Yes			3.05		CNV	MYC-activating
	SMO	Gain	Yes			3.14		CNV	SMO-activating
HPD6	TP53	p.A159F	Yes	Yes	Yes	33.01	53.64	SNV	TP53-inactivating
	KRAS	Gain	Yes	Yes	Yes	9.9	7.99	CNV	KRAS-activating
	MYC	Gain	Yes			3.02		CNV	MYC-activating

HPD, hyperprogressive disease; SNV, single nucleotide variation; CNV, copy number variation; VAF, variant allele frequency.

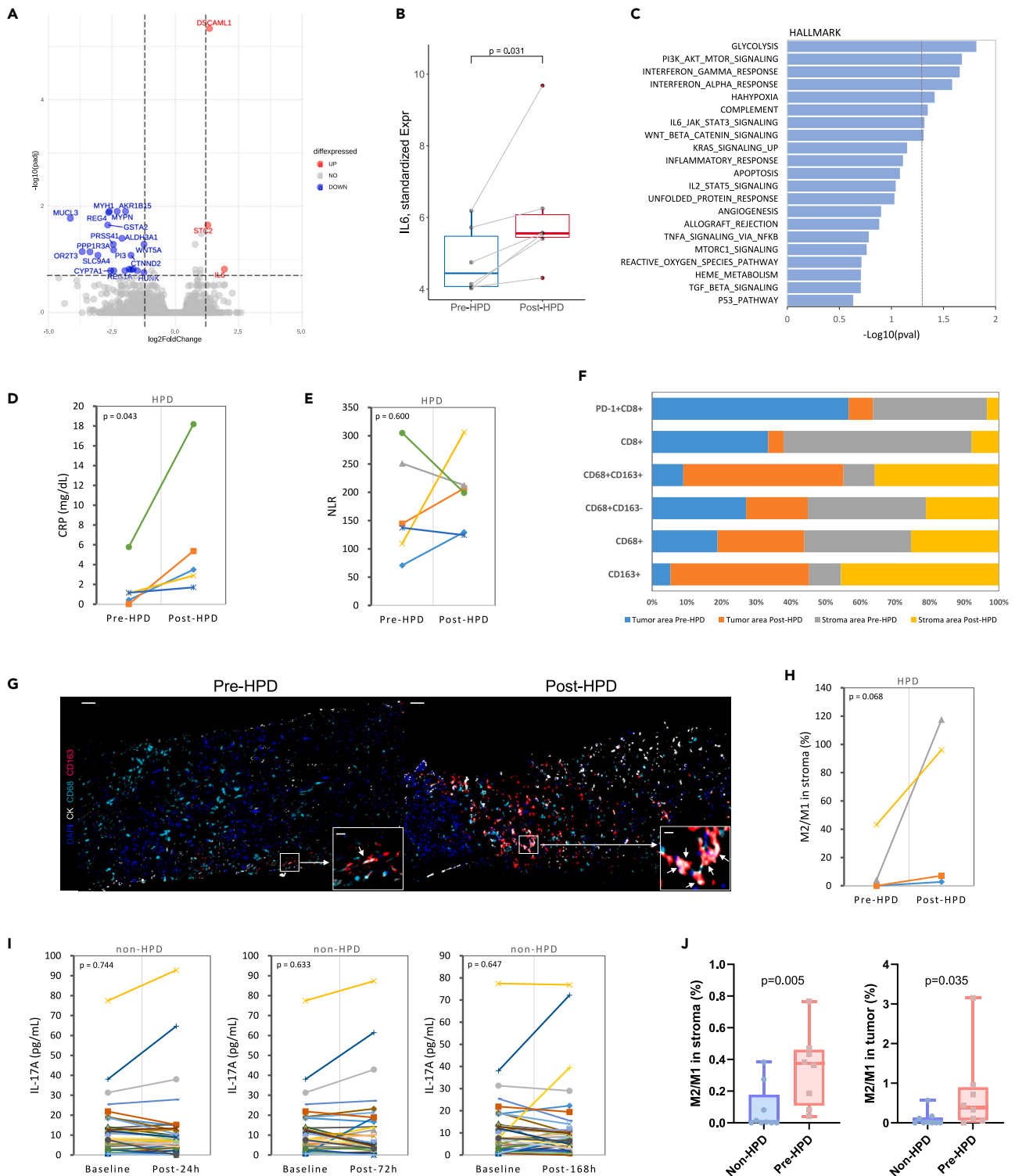


Figure 3. Gene expression and TiME features in paired HPD samples

(A) Significantly up- or down-regulated genes revealed by RNA-seq between pre- and post-HPD samples.

(B) IL6 expression in post-HPD samples compared with pre-HPD samples. The boxplot displays the standard five-number summary (Q1 – 1.5*IQR, Q1, Median, Q3 and Q3 + 1.5*IQR).

(C) Enrichment analysis of HPD-associated pathways revealed using ssGSEA.

(D) CRP levels in post-HPD samples compared with the pre-HPD samples.

Figure 3. Continued

(E) NLR levels in post-HPD samples compared with pre-HPD samples.

(F) The relative percentage of immune subsets in the TiME in HPD patients with paired samples by mIF.

(G) Representative images of mIF staining from pre- and post-HPD samples. Scale bars, 50 μm (main images) and 10 μm (insets). Arrowheads denote M2 macrophages (CD68⁺CD163⁺).

(H) M2/M1 ratio in the stromal area of the TiME by mIF in post-HPD samples compared with the pre-HPD samples.

(I) Dynamic change of IL-17A levels in post-24 h, 72 h, and 168 h compared with baseline samples of non-HPD liver cancer patients.

(J) M2/M1 ratio in the TiME by mIF in non-HPD samples compared with the HPD samples in liver cancer patients. Data are represented as median \pm SEM. HPD, hyperprogressive disease; TiME: tumor immune microenvironment; CRP: C-reactive protein; NLR: neutrophil-lymphocyte ratio; mIF, multiplex immunofluorescence; ssGSEA, single sample gene set enrichment analysis; M2: M2 macrophages (CD68⁺CD163⁺); M1: M1 macrophages (CD68⁺CD163⁻).

51.5, $p = 0.013$), than the non-HPD individuals (Figures S5A and S5B). To study the above-identified high-frequency genetic alterations in a general cancer population, we queried The Cancer Genome Atlas (TCGA) databases through cBioPortal. A total of 3564 patients had cancer types that matched those in our HPD group, and the mutation frequencies of *TP53* and *CNN2* were only 48% and 1.4%, respectively (Figure S5C).

We found that IL-6 expression increased during HPD occurrence, and the dynamic changes in cytokine levels as the non-HPD group were also primarily verified in a cohort of liver cancer patients who received combination immunotherapy from a phase 1b study. A total of 33 patients had blood samples that passed dynamic quality control and were available for serum cytokine detection of IL-17A, a cytokine with a similar function to IL-6. However, we did not observe a significant change of IL-17A in the non-HPD group at 24 h, 72 h, and 168 h after administration (Figure 3I).

For the TiME analysis, we collected baseline tissue samples from liver cancer patients treated with combined immunotherapy by mIF, including 9 non-HPD and 8 HPD patients (HPD5 and HPD6 had liver cancer and were included in this analysis). The results showed that the M2/M1 ratio was significantly higher in HPD samples than in non-HPD samples in both the stromal area (median, 0.373 vs. 0.005, $p = 0.005$) and the tumor area (median, 0.385 vs. <0.001 , $p = 0.035$, Figure 3J).

Salvage treatment strategies after HPD

Although all 6 patients received rescue therapy after HPD, 4 patients died within 3 months. The median overall survival (OS) of all patients was only 3.7 months (Figure 1B). Importantly, one patient (HPD3) with neuroendocrine urothelial carcinoma experienced HPD after a second-line pembrolizumab plus carboplatin treatment refractory to chemotherapy but responded to combined irinotecan plus bevacizumab (IB) treatment for 7 months (Figures 4A and 4B). However, the patient stopped IB due to new progression and died 12 months after HPD. Meanwhile, the change in neuron-specific enolase (NSE) levels was consistent with the tumor burden and treatment efficacy (Figure 4A). We identified in both pre- and post-HPD biopsies mutations in *TP53*, copy number gain of *CCNE1* and *MYC* (Table 2).

DISCUSSION

All six HPD patients received immunotherapy combined with either chemotherapy or an anti-angiogenic agent, indicating that HPD remains a pitfall of ICB combination therapy. To date, studies have mainly been focused on the description of clinical features and predictive parameters^{8,9,18} and have not yet provided a satisfactory explanation to characterize the molecular features and biological processes of HPD. In reported clinical cases, the presentation of patients with HPD varies greatly, from a slightly faster progression to an explosive accelerated pattern with extremely fast tumor growth. The increased tumor burden and increased TGR of the patients in our study were far beyond the criteria of HPD, which is considered an explosive pattern. Patients with this pattern of HPD, which is more invasive and is associated with worse survival outcomes, are potentially more valuable for mechanistic studies. Here, we obtained complete immunogenetic alteration data from paired samples from six HPD patients with explosive patterns through multiomics analysis and discovered several essential genetic and tumor environmental changes that may be related to HPD.

Tumor driver genes at the DNA level do not appear to be altered during the development of HPD. In our study, nearly all the main tumor driver gene mutations were preserved in the post-HPD specimens after such a rapid progression, and there was no significant change in tumor heterogeneity or TMB between the paired samples. These results indicate that the presence of preexisting molecular features, including genetic mutations, in baseline tumor tissues likely drives HPD occurrence after combined

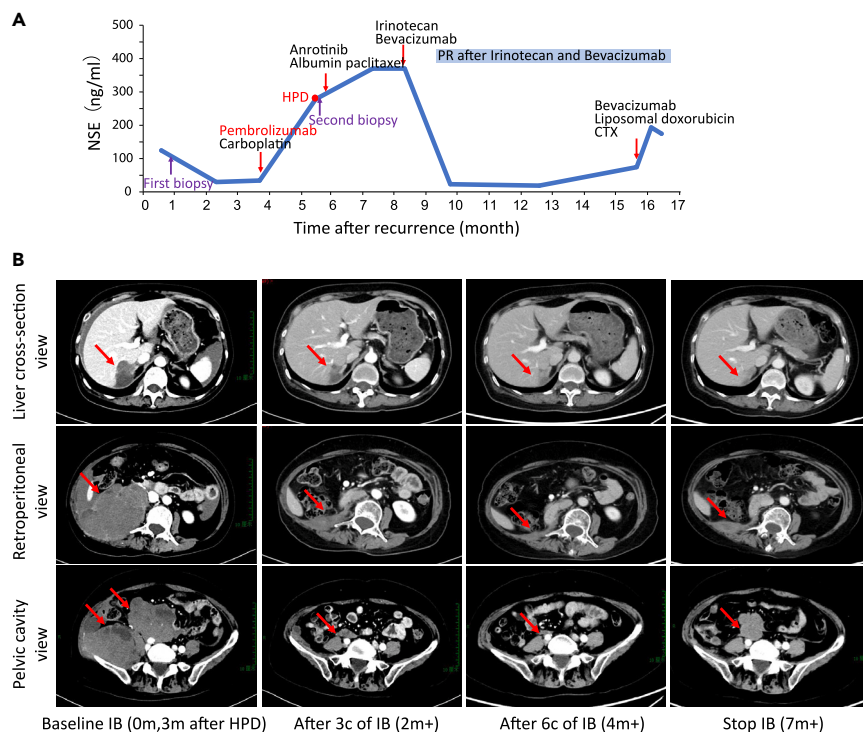


Figure 4. Dynamic tumor changes in one HPD patient with long survival

(A) Treatment timeline and dynamics of NSE levels. Red arrows indicate the starting time of treatments. Purple arrows indicate the time of biopsy performed.

(B) CT scans performed during the progression of the disease after IB treatment at the start of IB treatment, PR after 3 cycles, 6 cycles, and cessation of IB with slow progression after 10 cycles. The corresponding treatments and clinical events are labeled below the images. Upper rows: liver cross-section view; middle rows: retroperitoneal view; bottom rows: pelvic cavity view. HPD, hyperprogressive disease; NSE, neuron-specific enolase; IB, irinotecan plus bevacizumab therapy.

immunotherapy. Although the HPD patients had different cancer backgrounds, we found that the tumor suppressor gene *TP53* was altered in 100% (6/6); these mutations were all located inside the DBD, were predicted to be deleterious and truncating, and were present in both in pre- and post-HPD samples. Thus, these mutations likely disturb the cancer-mitigating functions of *TP53*. Previous studies have demonstrated that *MDM2/MDM4* and *EGFR* amplifications might be correlated with HPD.^{9,19} However, we did not observe *MDM2/MDM4* amplification in our cases, which occur upstream of *TP53* repression and can lead to HPD by disturbing *TP53* activity or functions. Furthermore, *TP53* mutations were found to be accompanied by increased immunosuppressive Treg cell and M2 macrophage infiltration in triple-negative breast cancer.²⁰ Mutation of another tumor suppressor gene, *VHL*, has also been reported to be involved in HPD after anti-PD-1 therapy by selection pressure.²¹ In addition, somatic mutations of *SMARCA4* and *CDKN2A*, and copy number gains of *FGF3/4/19*, *CCND1*, *MYC*, *KRAS*, and *ATK2* were also observed in paired pre- and post-HPD samples, and these genes are widely known to take part in cell proliferation and the cell cycle. Thus, the preexisting inactivation of critical suppressor genes and activation of oncogenes might be involved in HPD and may help recognize the process of HPD with immunotherapy.

We also analyzed the changes in gene expression in paired HPD samples, and the significant findings were interference in several key immune-related and cancer proliferation-related pathways that might be associated with HPD. Importantly, IL-6 expression was significantly elevated after HPD in all patients and these samples showed enrichment of immune function-related pathways including IL6/JAK/STAT3 signaling and the interferon gamma response pathways. However, IL-17A, a cytokine with a similar function to IL-6, was not similarly elevated in the non-HPD group after immunotherapy. IL-6, an immune inflammatory cytokine involved in immune cell development, has been shown to be associated with worse survival after treatment with anti-PD-1 therapy,^{22,23} poorer treatment response,²⁴ and higher risk of

immune-related adverse events.²⁵ IL-6 in the TiME is produced by cancer cells, host stromal cells, or tumor-infiltrating immune cells such as macrophages. Locally produced IL-6 can provide feedback and enhance the cancer-targeting functions of tumor-infiltrating macrophages and mediate epithelial-mesenchymal transition (EMT) via the JAK/STAT3 signaling pathway. IL6 probably promotes the generation of a tumor-suppressive TiME by interfering with the infiltration of CD8⁺ T cells and recruiting Treg cells, Th17 cells, M2 macrophages, and myeloid-derived suppressor cells (MDSCs).²⁶ Interestingly, the upregulation of IL-6 expression in cancer cells might result from mutations in *TP53* and consequent alterations in the JAK/STAT3 pathway. In many circumstances, locally produced IL-6 reaches the peripheral circulation and elicits systemic effects such as cachexia and paraneoplastic syndrome, including increased levels of CRP in serum, which was also observed in our HPD patients, resulting in the probable accumulation of MDSCs related to resistance to ICIs.⁸ In addition, upregulation of other immune checkpoint suppressor molecules, such as T-cell immunoglobulin mucin-3 (TIM-3) and immunosuppressive MDSCs, can lead to resistance to ICI treatment^{12,27} and might also promote HPD. These findings indicated that IL-6 might be involved in the immune depressive TiME of HPD.

Nevertheless, how ICI treatment stimulates HPD is a key question in HPD research. Some researchers discovered that the expression of intrinsic PD-1 in tumor cells, application of PD-1 antibody, or knockdown of PD-1 increased cell viability, while overexpression of PD-1 decreased cell proliferation, suggesting that PD-1 blockade itself may promote cancer growth under immunosuppressive conditions.²⁸ Recent studies further revealed that PD-1/PD-L1 expressed by the tumor cells themselves is an important regulator that inhibits tumor cell proliferation; however, this effect was relieved by PD-1/PD-L1 inhibitors.¹⁵ This inhibition reactivates the MAPK and PI3K signaling pathways and might promote HPD. It needs to be further investigated whether there is an interaction between autonomous PD-1/PD-L1 expression on the surface of tumor cells and/or other factors, such as IL-6, M2 macrophages, and CD8⁺ T cells. Our exploratory analysis of the TiME by mIF *in situ* also revealed potential immune depressive molecular features correlated with HPD, including a high M2/M1 ratio and low CD8⁺ T cell numbers. It has long been known that increased IL-6 levels, exhausted CD8⁺ T cells, and M2 macrophages, including CD163⁺ macrophages, are related to resistance to ICIs.²⁹ The infiltration of M2 macrophages (PD-L1⁺CD163⁺CD33⁺) in tumors induces HPD by Fc-Fcγ receptor binding.³⁰ In addition, IL-6 is reported to promote cancer progression via the BF-κB signaling pathway³¹; IL-6 has also been associated with tumor metastasis. Blocking IL-6 significantly decreased tumor progression and the number of M2 macrophages and improved the CD8⁺ T-cell response.³² Since IL-6 can be released by macrophages, T cells, and even tumor cells, it could be speculated that a vicious cycle of IL-6 secretion, M2 polarization, and CD8⁺ T-cell exhaustion ensues in HPD patients. Thus, the mechanisms underlying IL-6-induced M2 polarization are partially possible, and the potential treatment value for HPD patients should be further verified.

Management of HPD has always been challenging because there is no established patient screening marker or salvage treatment protocol. Here, one HPD patient responded well to the IB regimen for a prolonged period after failure to respond to albumin-bound paclitaxel plus anlotinib. Irinotecan (through its metabolite SN38) is a potent inhibitor of topoisomerase I, which relaxes DNA supercoils created during replication and transcription and is essential for DNA replication. Bevacizumab is an anti-VEGF antibody that blocks angiogenesis. Simultaneous blockade of neovascularization and DNA replication is expected to keep fast-growing tumors at bay and might be an effective salvage treatment strategy for HPD patients.

In conclusion, gene alterations in tumor driver genes seem to remain stable in the development of HPD. A suppressed TiME with a high M2/M1 ratio, elevated IL-6 expression levels, and high CRP levels was observed after HPD. These findings may help elucidate the mechanisms underlying HPD after combined immunotherapy, warranting further verification.

Limitations of the study

This study has several limitations. First, it was a retrospective study with limited sample size; therefore, future studies involving more patients and, ideally, a comparison with non-HPD patients are needed to validate our results. Second, the samples were from different cancer types, which were a limitation on the one hand but allowed us to search for common biological processes of HPD by paired analysis from each patient on the other hand. Finally, further studies are required to verify the discoveries in this study and to further elucidate the mechanisms underlying HPD.

STAR★METHODS

Detailed methods are provided in the online version of this paper and include the following:

- KEY RESOURCES TABLE
- RESOURCE AVAILABILITY
 - Lead contact
 - Materials availability
 - Data and code availability
- EXPERIMENTAL MODEL AND SUBJECT DETAILS
 - Human subjects and clinical protocol
- METHOD DETAILS
 - Multiplex immunofluorescence
 - Bead-based immunoassay
 - Genetic analysis
- QUANTIFICATION AND STATISTICAL ANALYSIS
- ADDITIONAL RESOURCES

SUPPLEMENTAL INFORMATION

Supplemental information can be found online at <https://doi.org/10.1016/j.isci.2023.106720>.

ACKNOWLEDGMENTS

The authors are grateful to the patients for participating in this study and to their families for allowing the publication of the results. In addition, the authors would like to thank The Cancer Genome Atlas Research Network (TCGA), and the MSKCC cBioPortal for providing cancer genomic and transcriptomic data and analytical tools (TIMER2.0, PATHER, and KEGG). We would like to thank the developers of an online gene mutation pathogenic prediction tool for CADD (<https://cadd.gs.washington.edu>). Graphical abstract was created with figdraw.com. The authors wish to thank Pr. Xiaoyan Qiu from the Department of Immunology, Peking University Health Sciences Center, and our colleague Lin Feng from the Department of Immunology, National Cancer Center/National Clinical Research Center for Cancer/Cancer Hospital for their helpful discussions and suggestions. This work was funded by Beijing Hope Run Special Fund of Cancer Foundation of China (grant No. LC 2020B16), Cultivation project of Medical Oncology Key Foundation of Cancer Hospital Chinese Academy of Medical Sciences (grant No. CICAMS-MOCP2022011), Beijing Natural Science Foundation (grant No. L222101) and CAMS Innovation Fund for Medical Sciences (CIFMS) (grant No. 2021-I2M-1-066). This study is also supported by BeiGene (Beijing) Co., Ltd.

AUTHOR CONTRIBUTIONS

A.P.Z. and C.F.G. conceived the project and designed the experiments. A.P.Z., W.Z., Y.K.S., C.F.G., Z.C.J., and J.Z.S. contributed to patient enrollment and related sample/data analysis. C.F.G. conducted the experiments and acquired the data. C.F.G., Y.S., and S.H.W. analyzed the data. C.F.G., T.Y.L., and J.L. wrote the manuscript. A.P.Z. supervised the project. All authors discussed the results and revised the manuscript.

DECLARATION OF INTERESTS

The authors declare no conflicts of interest.

INCLUSION AND DIVERSITY

We support inclusive, diverse, and equitable conduct of research.

Received: October 25, 2022

Revised: January 31, 2023

Accepted: April 19, 2023

Published: April 23, 2023

REFERENCES

1. Champiat, S., Derclé, L., Ammari, S., Massard, C., Hollebecque, A., Postel-Vinay, S., Chaput, N., Eggermont, A., Marabelle, A., Soria, J.C., and Ferté, C. (2017). Hyperprogressive disease is a new pattern of progression in cancer patients treated by anti-PD-1/PD-L1. *Clin. Cancer Res.* 23, 1920–1928. <https://doi.org/10.1158/1078-0432.CCR-16-1741>.
2. Borcoman, E., Kanjanapan, Y., Champiat, S., Kato, S., Servois, V., Kurzrock, R., Goel, S., Bedard, P., and Le Tourneau, C. (2019). Novel patterns of response under immunotherapy. *Ann. Oncol.* 30, 385–396. <https://doi.org/10.1093/annonc/mdz003>.
3. Ferrara, R., Mezquita, L., Texier, M., Lahmar, J., Audigier-Valette, C., Tessonier, L., Mazieres, J., Zalcman, G., Brosseau, S., Le Moulec, S., et al. (2018). Hyperprogressive disease in patients with advanced non-small cell lung cancer treated with PD-1/PD-L1 inhibitors or with single-agent chemotherapy. *JAMA Oncol.* 4, 1543–1552. <https://doi.org/10.1001/jamaoncol.2018.3676>.
4. Saâda-Bouزيد, E., Defaucheux, C., Karabajakian, A., Coloma, V.P., Servois, V., Paoletti, X., Even, C., Fayette, J., Guigay, J., Lohat, D., et al. (2017). Hyperprogression during anti-PD-1/PD-L1 therapy in patients with recurrent and/or metastatic head and neck squamous cell carcinoma. *Ann. Oncol.* 28, 1605–1611. <https://doi.org/10.1093/annonc/mdx178>.
5. Park, H.J., Kim, K.W., Won, S.E., Yoon, S., Chae, Y.K., Tirumani, S.H., and Ramaiya, N.H. (2021). Definition, incidence, and challenges for assessment of hyperprogressive disease during cancer treatment with immune checkpoint inhibitors: a systematic review and meta-analysis. *JAMA Netw. Open* 4, e211136. <https://doi.org/10.1001/jamanetworkopen.2021.1136>.
6. Zheng, Z., Wu, K., Yao, Z., Mu, X., Wu, H., Zhao, W., Cheng, L., and Liu, Z. (2020). Hyperprogressive disease in patients with advanced renal cell carcinoma: a new pattern of post-treatment cancer behavior. *Immunol. Res.* 68, 204–212. <https://doi.org/10.1007/s12026-020-09138-4>.
7. Kanjanapan, Y., Day, D., Wang, L., Al-Sawaihey, H., Abbas, E., Namini, A., Siu, L.L., Hansen, A., Razak, A.A., Spreafico, A., et al. (2019). Hyperprogressive disease in early-phase immunotherapy trials: clinical predictors and association with immune-related toxicities. *Cancer* 125, 1341–1349. <https://doi.org/10.1002/cncr.31999>.
8. Sasaki, A., Nakamura, Y., Mishima, S., Kawazoe, A., Kuboki, Y., Bando, H., Kojima, T., Doi, T., Ohtsu, A., Yoshino, T., et al. (2019). Predictive factors for hyperprogressive disease during nivolumab as anti-PD1 treatment in patients with advanced gastric cancer. *Gastric Cancer* 22, 793–802. <https://doi.org/10.1007/s10120-018-00922-8>.
9. Kato, S., Goodman, A., Walavalkar, V., Barkauskas, D.A., Sharabi, A., and Kurzrock, R. (2017). Hyperprogressors after immunotherapy: analysis of genomic alterations associated with accelerated growth rate. *Clin. Cancer Res.* 23, 4242–4250. <https://doi.org/10.1158/1078-0432.CCR-16-3133>.
10. Wang, W., Wu, M., Liu, M., Yan, Z., Wang, G., Mao, D., and Wang, M. (2020). Hyperprogression to camrelizumab in a patient with esophageal squamous cell carcinoma harboring EGFR kinase domain duplication. *J. Immunother. Cancer* 8, e000793. <https://doi.org/10.1136/jitc-2020-000793>.
11. Kim, C.G., Kim, K.H., Pyo, K.H., Xin, C.F., Hong, M.H., Ahn, B.C., Kim, Y., Choi, S.J., Yoon, H.I., Lee, J.G., et al. (2019). Hyperprogressive disease during PD-1/PD-L1 blockade in patients with non-small-cell lung cancer. *Ann. Oncol.* 30, 1104–1113. <https://doi.org/10.1093/annonc/mdz123>.
12. Koyama, S., Akbay, E.A., Li, Y.Y., Herter-Sprrie, G.S., Buczkowski, K.A., Richards, W.G., Gandhi, L., Redig, A.J., Rodig, S.J., Asahina, H., et al. (2016). Adaptive resistance to therapeutic PD-1 blockade is associated with upregulation of alternative immune checkpoints. *Nat. Commun.* 7, 10501. <https://doi.org/10.1038/ncomms10501>.
13. Wang, X., Wang, F., Zhong, M., Yarden, Y., and Fu, L. (2020). The biomarkers of hyperprogressive disease in PD-1/PD-L1 blockage therapy. *Mol. Cancer* 19, 81. <https://doi.org/10.1186/s12943-020-01200-x>.
14. Kamada, T., Togashi, Y., Tay, C., Ha, D., Sasaki, A., Nakamura, Y., Sato, E., Fukuoka, S., Tada, Y., Tanaka, A., et al. (2019). PD-1(+) regulatory T cells amplified by PD-1 blockade promote hyperprogression of cancer. *Proc. Natl. Acad. Sci. USA* 116, 9999–10008. <https://doi.org/10.1073/pnas.1822001116>.
15. Wang, X., Yang, X., Zhang, C., Wang, Y., Cheng, T., Duan, L., Tong, Z., Tan, S., Zhang, H., Saw, P.E., et al. (2020). Tumor cell-intrinsic PD-1 receptor is a tumor suppressor and mediates resistance to PD-1 blockade therapy. *Proc. Natl. Acad. Sci. USA* 117, 6640–6650. <https://doi.org/10.1073/pnas.1921445117>.
16. Nakagomi, H., Mochizuki, H., Inoue, M., Hirotsu, Y., Amemiya, K., Sakamoto, I., Nakagomi, S., Kubota, T., and Omata, M. (2018). Combined annotation-dependent depletion score for BRCA1/2 variants in patients with breast and/or ovarian cancer. *Cancer Sci.* 109, 453–461. <https://doi.org/10.1111/cas.13464>.
17. Charoentong, P., Finotello, F., Angelova, M., Mayer, C., Efremova, M., Rieder, D., Hackl, H., and Trajanoski, Z. (2017). Pan-cancer immunogenomic analyses reveal Genotype-immunophenotype relationships and predictors of response to checkpoint blockade. *Cell Rep.* 18, 248–262. <https://doi.org/10.1016/j.celrep.2016.12.019>.
18. Zhang, L., Wu, L., Chen, Q., Zhang, B., Liu, J., Liu, S., Mo, X., Li, M., Chen, Z., Chen, L., et al. (2021). Predicting hyperprogressive disease in patients with advanced hepatocellular carcinoma treated with anti-programmed cell death 1 therapy. *EClinicalMedicine* 31, 100673. <https://doi.org/10.1016/j.eclinm.2020.100673>.
19. Adashek, J.J., Subbiah, I.M., Matos, I., Garralda, E., Menta, A.K., Ganeshan, D.M., and Subbiah, V. (2020). Hyperprogression and immunotherapy: fact, fiction, or alternative fact? *Trends Cancer* 6, 181–191. <https://doi.org/10.1016/j.trecan.2020.01.005>.
20. Oshi, M., Asaoka, M., Tokumaru, Y., Angarita, F.A., Yan, L., Matsuyama, R., Zsiros, E., Ishikawa, T., Endo, I., and Takabe, K. (2020). Abundance of regulatory T cell (Treg) as a predictive biomarker for neoadjuvant chemotherapy in triple-negative breast cancer. *Cancers* 12, 3038. <https://doi.org/10.3390/cancers12103038>.
21. Xiong, D., Wang, Y., Singavi, A.K., Mackinnon, A.C., George, B., and You, M. (2018). Immunogenomic landscape contributes to hyperprogressive disease after anti-PD-1 immunotherapy for cancer. *iScience* 9, 258–277. <https://doi.org/10.1016/j.isci.2018.10.021>.
22. Carril-Ajuria, L., Desnoyer, A., Meylan, M., Dalban, C., Naigeon, M., Cassard, L., Vano, Y., Rioux-Leclercq, N., Chouaib, S., Beuselinck, B., et al. (2022). Baseline circulating unswitched memory B cells and B-cell related soluble factors are associated with overall survival in patients with clear cell renal cell carcinoma treated with nivolumab within the NIVOREN GETUG-AFU 26 study. *J. Immunother. Cancer* 10, e004885. <https://doi.org/10.1136/jitc-2022-004885>.
23. Laino, A.S., Woods, D., Vassallo, M., Qian, X., Tang, H., Wind-Rotolo, M., and Weber, J. (2020). Serum interleukin-6 and C-reactive protein are associated with survival in melanoma patients receiving immune checkpoint inhibition. *J. Immunother. Cancer* 8, e000842. <https://doi.org/10.1136/jitc-2020-000842>.
24. Wang, Y., Ramachandran, V., Sui, D., Xu, K., Haydu, L.E., Fang, S., McQuade, J.L., Fisher, S.B., Lucci, A., Keung, E.Z., et al. (2022). Evaluation of plasma IL-6 in patients with melanoma as a prognostic and checkpoint immunotherapy predictive biomarker. *J. Invest. Dermatol.* 142, 2046–2049.e3. <https://doi.org/10.1016/j.jid.2021.12.012>.
25. Gérard, A., Doyen, J., Cremoni, M., Bailly, L., Zorzi, K., Ruetsch-Chelli, C., Brglez, V., Picard-Gauci, A., Troin, L., Esnault, V.L.M., et al. (2021). Baseline and early functional immune response is associated with subsequent clinical outcomes of PD-1 inhibition therapy in metastatic melanoma

- patients. *J. Immunother. Cancer* 9, e002512. <https://doi.org/10.1136/jitc-2021-002512>.
26. Hailemichael, Y., Johnson, D.H., Abdel-Wahab, N., Foo, W.C., Bentebibel, S.E., Daher, M., Haymaker, C., Wani, K., Saberian, C., Ogata, D., et al. (2022). Interleukin-6 blockade abrogates immunotherapy toxicity and promotes tumor immunity. *Cancer Cell* 40, 509–523.e6. <https://doi.org/10.1016/j.ccell.2022.04.004>.
 27. Mojsilovic, S., Mojsilovic, S.S., Bjelica, S., and Santibanez, J.F. (2021). Transforming growth factor-beta1 and myeloid-derived suppressor cells: a cancerous partnership. *Dev. Dyn.* <https://doi.org/10.1002/dvdy.339>.
 28. Du, S., McCall, N., Park, K., Guan, Q., Fontina, P., Ertel, A., Zhan, T., Dicker, A.P., and Lu, B. (2018). Blockade of tumor-expressed PD-1 promotes lung cancer growth. *Oncolmunology* 7, e1408747. <https://doi.org/10.1080/2162402x.2017.1408747>.
 29. Kuo, I.Y., Yang, Y.E., Yang, P.S., Tsai, Y.J., Tzeng, H.T., Cheng, H.C., Kuo, W.T., Su, W.C., Chang, C.P., and Wang, Y.C. (2021). Converged Rab37/IL-6 trafficking and STAT3/PD-1 transcription axes elicit an immunosuppressive lung tumor microenvironment. *Theranostics* 11, 7029–7044. <https://doi.org/10.7150/thno.60040>.
 30. Lo Russo, G., Moro, M., Sommariva, M., Cancila, V., Boeri, M., Centonze, G., Ferro, S., Ganzinelli, M., Gasparini, P., Huber, V., et al. (2019). Antibody-fc/FcR interaction on macrophages as a mechanism for hyperprogressive disease in non-small cell lung cancer subsequent to PD-1/PD-L1 blockade. *Clin. Cancer Res.* 25, 989–999. <https://doi.org/10.1158/1078-0432.CCR-18-1390>.
 31. Qin, X., Yan, M., Wang, X., Xu, Q., Wang, X., Zhu, X., Shi, J., Li, Z., Zhang, J., and Chen, W. (2018). Cancer-associated fibroblast-derived IL-6 promotes head and neck cancer progression via the osteopontin-NF-kappa B signaling pathway. *Theranostics* 8, 921–940. <https://doi.org/10.7150/thno.22182>.
 32. Caetano, M.S., Zhang, H., Cumpian, A.M., Gong, L., Unver, N., Ostrin, E.J., Daliri, S., Chang, S.H., Ochoa, C.E., Hanash, S., et al. (2016). IL6 blockade reprograms the lung tumor microenvironment to limit the development and progression of K-ras-Mutant lung cancer. *Cancer Res.* 76, 3189–3199. <https://doi.org/10.1158/0008-5472.Can-15-2840>.

STAR★METHODS

KEY RESOURCES TABLE

REAGENT or RESOURCE	SOURCE	IDENTIFIER
Antibodies		
Anti-CD163	Abcam	Cat#ab182422; RRID: AB_2753196
Anti-CD8	Abcam	Cat# ab178089; RRID: AB_2756374
Anti-CD68	Abcam	Cat#ab213363; RRID: AB_2801637
Anti-PD-1	Cell Signaling Technology	Cat#86183S
Anti-PD-L1	Cell Signaling Technology	Cat#13684S
Anti-panCK	Abcam	Cat#ab7753; RRID: AB_306047
Biological samples		
Cancer patient blood	Cancer Hospital, Chinese Academy of Medical Sciences	This paper
Cancer patient specimen	Cancer Hospital, Chinese Academy of Medical Sciences	This paper
Critical commercial assays		
MagMAX FFPE DNA/RNA Ultra kit	ThermoFisher	Cat# A31881
Maxwell RSC blood DNA kit	Promega	Cat# AS1400
Opal automation mIF detection kit	Akoya	This paper
ProcartaPlex Human Cytokine/Chemokine/Growth Factor Panel	Affymetrix Inc.	This paper
ProcartaPlex Human Immuno-Oncology Checkpoint Panel	Affymetrix Inc.	This paper
Deposited data		
Original code	This paper	https://github.com/biosunsci/HPD_ZhouAP
Software and algorithms		
R programming language, v4.1.2	R Core Team	https://www.R-project.org/
R package, clusterProfiler, v4.2.2	Clustering	https://bioconductor.org/packages/clusterProfiler/
R package, DESeq2, v1.34.0	Normalization, Diff. Expr. analysis	https://bioconductor.org/packages/DESeq2/
R package, dplyr, v1.0.10	Tidyverse toolkit	https://CRAN.R-project.org/package=dplyr
R package, forcats, v0.5.2	Tidyverse toolkit	https://CRAN.R-project.org/package=forcats
R package, formatR, v0.5.2	Tidyverse toolkit	https://CRAN.R-project.org/package=formatR
R package, GenomeInfoDb, v1.30.1	Genomic tools	https://bioconductor.org/packages/GenomeInfoDb
R package, GenomicRanges, v1.46.1	Genomic tools	http://www.ploscompbiol.org/article/info%3Adoi%2F10.1371%2Fjournal.pcbi.1003118
R package, ggfortify, v0.4.15	Plot, format plots	https://CRAN.R-project.org/package=ggfortify
R package, ggplot2, v3.4.0	Plot, tidyverse toolkit	https://ggplot2.tidyverse.org
R package, ggpubr, v0.5.0	plot, arrange plots	https://CRAN.R-project.org/package=ggpubr
R package, ggsci, v2.9	Color themes	https://CRAN.R-project.org/package=ggsci
R package, GSEA, v1.42.0	GSEA analysis	http://www.biomedcentral.com/1471-2105/14/7
R package, IRanges, v2.28.0	Genomic tools	http://www.ploscompbiol.org/article/info%3Adoi%2F10.1371%2Fjournal.pcbi.1003118
R package, maftools, v2.8.05	Analysis and plot mutations	https://github.com/PoisonAlien/maftools

(Continued on next page)

Continued

REAGENT or RESOURCE	SOURCE	IDENTIFIER
R package, magrittr, v2.0.3	Basic tools	https://CRAN.R-project.org/package=magrittr
R package, MatrixGenerics, v1.6.0	Tools	https://bioconductor.org/packages/MatrixGenerics
R package, matrixStats, v0.63.0	Tools	https://CRAN.R-project.org/package=matrixStats
R package, openxlsx, v4.2.5.1	Tools	https://CRAN.R-project.org/package=openxlsx
R package, org.Hs.eg.db, v3.14.0	Ref DB	https://bioconductor.org/packages/org.Hs.eg.db/
R package, purrr, v1.0.1	Tidyverse toolkit	https://CRAN.R-project.org/package=purrr
R package, RColorBrewer, v1.1-3	Color picker	https://CRAN.R-project.org/package=RColorBrewer
R package, readr, v2.1.3	Tidyverse toolkit	https://CRAN.R-project.org/package=readr
R package, scales, v1.2.1	Value formatting	https://CRAN.R-project.org/package=scales
R package, stringr, v1.5.0	Tidyverse toolkit	https://CRAN.R-project.org/package=stringr
R package, survival, v3.5-0	Survival analysis	https://CRAN.R-project.org/package=survival
R package, survminer, v0.4.9	Survival analysis	https://rpkgs.datanovia.com/survminer/index.html
R package, tibble, v3.1.8	Tidyverse toolkit	https://CRAN.R-project.org/package=tibble
R package, tidyr, v1.2.1	Tidyverse toolkit	https://CRAN.R-project.org/package=tidyr
ExomeCNV	CNV calling	https://academic.oup.com/bioinformatics/article/27/19/2648/231564
Sentieon, Version 201911	SNV & Indel calling	https://www.sentieon.com/
VEP	Mutation annotation	https://useast.ensembl.org/info/docs/tools/vep/index.html
BWA	Reads aligning	https://github.com/lh3/bwa
Samtools	Sequence Viewer	http://www.htslib.org/
STAR, v2.7	Spliced Transcripts Alignment	https://github.com/alexdobin/STAR
STAR-Fusion	Identify gene-fusions from transcriptome	https://github.com/STAR-Fusion/STAR-Fusion
StringTie, v2.06	Transcriptome alignment, gene expression level estimation	https://ccb.jhu.edu/software/stringtie/#overview
Ucsc.hg19	Ref Genome	https://hgdownload.soe.ucsc.edu/downloads.html

RESOURCE AVAILABILITY**Lead contact**

Further information and any related requests should be directed to and will be fulfilled by the lead contact, Aiping Zhou (aiping_zhou@yeah.net).

Materials availability

This study did not generate new unique reagents.

Data and code availability

All original code generated as part of this study has been deposited at https://github.com/biosunsci/HPD_ZhouAP. A link to code has been included in the [key resources table](#). Any additional information required to the data reported in this work is available from the [lead contact](#) upon reasonable request.

EXPERIMENTAL MODEL AND SUBJECT DETAILS**Human subjects and clinical protocol**

Candidate patients were identified by screening hospital records from January 2019 to December 2021 according to the following criteria: advanced solid malignant tumor; received anti-PD-1/PD-L1 combination treatment; legible images for HPD evaluation; paired specimens available, and available baseline WES data. The treatment responses and tumor growth dynamics were independently assessed by oncologists and radiologists. Overall survival (OS) was defined as the time from the start of immunotherapy until death.

TTF was defined as the time from the start of immunotherapy until disease progression or the termination of treatment for any reason. Tumor volume change was defined as the tumor diameter calibrated change in the sum of the target lesions according to RECIST 1.1 criteria. This study was approved by the Institutional Ethics Committee of Cancer Hospital, Chinese Academy of Medical Sciences, Approval No. 21/099–2770. Six HPD (age of 47–67 years, 3 male and 3 female) and 24 non-HPD (age of 39–85 years, 14 male and 10 female) patients with stage IV solid cancer patients were included in the final analysis. Detailed information on clinical cohorts are depicted in [Tables 1](#) and [S4](#). Another non-HPD cohort of 33 advanced liver cancer patients (age of 38–75 years, 27 male and 6 female) who received combination immunotherapy (sintilimab plus bevacizumab biosimilar) with IL-17A cytokine were from a phase 1b study (approved by the Ethics Committee of the Cancer Hospital, Chinese Academy of Medical Sciences, Approval No. 18-126/1704).

METHOD DETAILS

Multiplex immunofluorescence

Formalin-fixed paraffin-embedded tumor tissue paired slides were prepared. Samples were stained using an Opal automation mIF detection kit (Akoya, Tokyo, Japan). A total of 6 markers were labeled in one seven-color multiplex panel. The following antibodies were used for one panel: anti-CD163 (Abcam Cat#ab182422), anti-CD8 (Abcam Cat# ab178089), anti-CD68 (Abcam Cat#ab213363), anti-PD-1 (Cell Signaling Technology Cat#86183S), anti-PD-L1 (Cell Signaling Technology Cat#13684S), and anti-panCK (Abcam Cat#ab7753). The labeled slides were scanned using a Vectra Polaris Automated Quantitative Pathology Imaging System (Akoya), and images from different channels were false-colored and superimposed. Tumor and stromal areas were divided based on CK-labeled tumor cells, and the cell nuclei were counterstained with 4'–6'-diamidino-2-phenylindole (DAPI). The results are reported as percentages (immune subset cells/total cells of DAPI) and density (cells/mm²) of each individual cell subpopulation in the tumor or stromal area.

Bead-based immunoassay

Peripheral blood samples (4 mL) were collected during study treatment (baseline, post-24h, post-72h, and post-168h) into a BD vacutainer blood collection tube (BD Biosciences, Franklin Lakes, NJ, USA) by venipuncture and centrifuged (1,000 g for 15 min) to isolate the serum. Multiple serological cytokine, including IL-17A, were simultaneously measured in serum samples using the ProcartaPlex Human Cytokine/Chemokine/Growth Factor Panel (Affymetrix Inc., Santa Clara, CA, USA) and the ProcartaPlex Human Immuno-Oncology Checkpoint Panel (Affymetrix Inc.).

Genetic analysis

DNA and RNA were extracted from paraffin-embedded (FFPE) or snap-frozen tissue with commercial kits [MagMAX FFPE DNA/RNA Ultra (ThermoFisher, Cat# A31881) or Maxwell RSC blood DNA (Promega, Cat# AS1400)], converted to sequencing libraries and sequenced on an Illumina platform. BWA/Sentieon (for WES) or STAR/StringTie2 (for RNA-seq) pipelines were used for the read alignment, assembly, and genetic analysis. The sequencing depth was ~285x for tumors and ~150x for normal cells for WES, and ~180 million aligned reads in the RNA-seq. The average sequencing depth of coverage was over 186.7x, with >20x at >97.2% exons. Somatic mutations were determined by comparing the tumor and paired peripheral whole blood samples and filtered and annotated using the Variant Effect Predictor (VEP) package. During CNV determination, a standard normal distribution was used to reduce bias, including the size of exonic regions, batch effect, quantity and quality of the sequencing data, local GC content, and genomic mappability. Considering the tumor heterogeneity and the tumor purity (tumor cell proportion in all samples was approximately 50.0%), genes with haploid copy number ≥ 3 or ≤ 1.2 were defined as copy number gain or loss, respectively. Oncodriver genes were annotated by referring to the online knowledge databases CKB (<https://ckbhome.jax.org/>) and OncoKB (<https://www.oncokb.org>). For RNA-seq, reads that passed the quality check were aligned to the hg19 reference genome using STAR Method (RRID: SCR_004463) and assembled using StringTie2 (version 1.3.5).

QUANTIFICATION AND STATISTICAL ANALYSIS

Analysis of paired data between pre- and post-HPD samples was performed using the Wilcoxon signed-rank test with a false discovery rate (FDR) correction where needed. Differentially expressed gene (DEG) analysis was performed with the DESeq2 (RRID: SCR_000154) method using read counts from RNA-seq. Up-regulated genes were screened as $P < 0.01$, $\log_{2}FC > 1$ and $\text{Padj} < 0.2$, and downregulated genes were

screened as $P < 0.01$, $\log_{2}FC < -1$ and $P_{adj} < 0.2$. Gene enrichment and biological pathway analyses were performed with single sample gene set enrichment analysis (ssGSEA) by using the hallmark gene sets and setting $P < 0.05$ and $P_{adj} < 0.2$ as the enrichment significance considerations. Differences between HPD and non-HPD groups for parameters were determined by using the Mann-Whitney U test (unpaired, nonparametric, two-tailed). Categorical data were analyzed using two-sided Fisher's exact test. Statistical analyses and data visualization were performed using R version 4.1 software. Unless stated otherwise, all P values were two-sided, with an α of 0.05.

ADDITIONAL RESOURCES

This work is part of a clinical trial which has been registered on [ClinicalTrials.gov](https://clinicaltrials.gov/ct2/show/NCT04072679) (Identifier: NCT04072679, <https://clinicaltrials.gov/ct2/show/NCT04072679>).